ACS APPLIED MATERIALS & INTERFACES

Research Article

Cite This: ACS Appl. Mater. Interfaces 2019, 11, 36259−36269

www.acsami.org

Biofriendly and Regenerable Emotional Monitor from Interfacial Ultrathin 2D PDA/AuNPs Cross-linking Films

Liming Chen,[‡,§] Youju Huang,[*,†,§,#] Liping Song,[§] Wuliang Yin,[‡] Linxi Hou,[⊥] Xuqing Liu,[*,∥] and Tao Chen[*,§]

[†]College of Materials, Chemistry and Chemical Engineering, Hangzhou Normal University, Hangzhou, Zhejiang 311121, China

[‡]Department of Electrical and Electronic Engineering and [∥]Department of Materials, University of Manchester, Sackville Street Building, Manchester M13 9PL, U.K.

[§]Ningbo Institute of Material Technology and Engineering, Key Laboratory of Graphene Technologies and Applications of Zhejiang Province, Chinese Academy of Sciences, Ningbo 315201, China

[⊥]Department of Materials-Oriented Chemical Engineering, College of Chemical Engineering, Fuzhou University, 2 Xueyuan Road, Fuzhou 350108, China

[#]National Engineering Research Centre for Advanced Polymer Processing Technology, Key Laboratory of Materials Processing and Mold (Zhengzhou University), Ministry of Education, Zhengzhou University, Zhengzhou 450002, P. R. China

Supporting Information

ABSTRACT: Well-designed 2D materials with ultrathin structures show great potential for humidity-sensing performance owing to their high surface-volume ratio and a great number of exposed atoms on the surface. However, some sensing elements employed for healthcare applications may be considered as potentially risky, such as inflammation, granuloma formation, and carcinogenesis. Herein, we explored biofriendly humidity-sensing characteristics inspired by the great biocompatibility and conductivity of hyperbranched polyethyleneimine-capped gold nanoparticles and cross-linked with polydopamine from the adhesive proteins in mussels. It was successfully employed into two kinds of wearable devices, sports watches and breathing masks, for real-time recording humidity's fluctuation in expiration and sweat with changes of individual's crying, laughing, nervous, sleeping, training, and cold states. The wearable devices allow us to monitor individual's physical activities and emotional states well, suggesting a promising prospect in safe, reusable, long term, and noncontact human health monitoring applications.

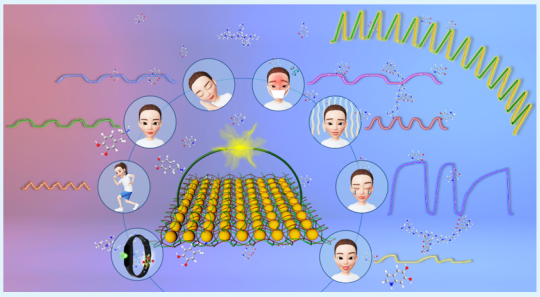

KEYWORDS: *gold nanoparticles, dopamine, humidity sensor, sports watch, emotional monitoring*

INTRODUCTION

Wearable microelectronics with superior sensing capabilities have presented great promising potential to be next-generation electronics.[1−4] They are promoted significantly by huge demands for diverse applications, including biological recognition,[5] disease diagnosis,[6] and everyday health monitoring.[7,8] However, most wearable electronics are touch-sensing devices for collecting individual's signals (such as temperature, heart rate, sweat, and respiration).[9−13] This is likely to cause cracks or damages in sensing materials, and thus fail to provide a deep insight into the detection of individual's gas molecular state diffusive from human body in a longer range. Some touch-sensors are uncomfortable to human skin and may cause and retain their allergenic reactivity. Therefore, it is extremely significant to explore noncontact sensitive materials. Moisture is an ideal candidate of signal source to realize noncontact and long range induction because water (∼66% of body weight) plays an extremely important role in most of human's metabolism processes and physiological activities.[14] Obviously, the realization of noncontact electronics indeed require the sensing materials to have an ultrathin structure (high surface-volume ratio) with great interior competence to absorb water molecules and efficiently record dynamic signals from surrounding environment.[15]

Well-designed 2D materials with adequate conductive atoms present highly carrier mobility for the selective absorption of water molecules. For instance, 2D graphene has proved to be a promising material candidate for sensitive humidity detection because of good conductivity and high charge carrier mobility.[7,16,17] Few-layer 2D black phosphorus presents stable and selective humidity-sensing behavior.[18,19] Electronic circuits based on the monolayers of gold nanoparticles (AuNPs) functionalized with charged organic ligands was fabricated as a humidity-sensing unit.[2] However, because the change of resistance is not abrupt and the sensing mechanism is also unclear, traditional sensing materials usually exhibit a low

Received: July 8, 2019
Accepted: September 10, 2019
Published: September 10, 2019

DOI: 10.1021/acsami.9b11918
ACS Appl. Mater. Interfaces 2019, 11, 36259−36269

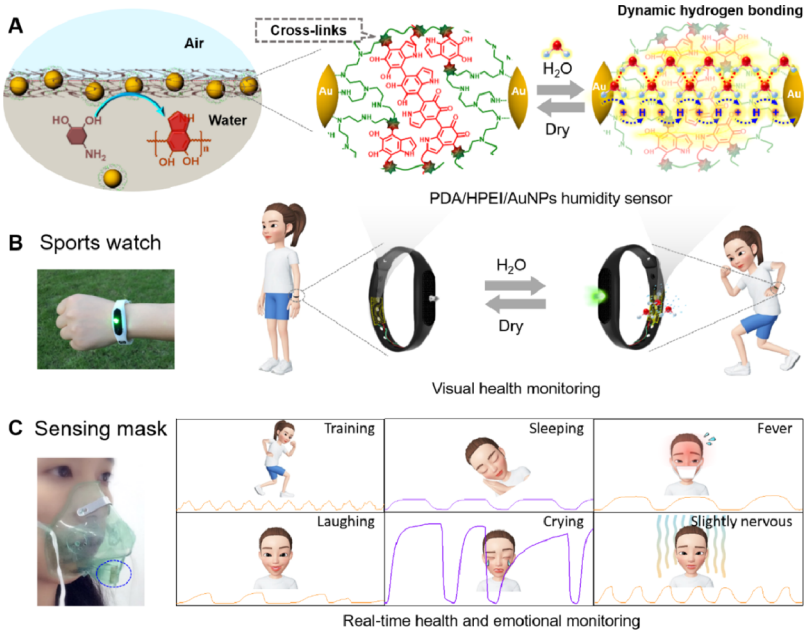

Figure 1. (A) Overall schematic of a humidity sensor based on PDA/HPEI/AuNPs film, which is sensitive under dry and humid conditions with an electronic circuit, (B) designed sports watch for detecting RH change on human skin surface switched by sweat and laser radiation and (C) the breath sensor for monitoring different physical and emotional activities (including training, sleeping, healthy states, laughing, crying, and nervous state).

sensitivity or/and response rate, which prevent applications for real-time physiological and psychological monitoring. So far, several efforts have been devoted to construct distinctive structures as ultrafast humidity sensors for respiratory monitoring, such as the fabricating graphene-polymer system,[20] introducing supramolecular polymers (nanofibers),[21] designing functionalized carbon nanotubes,[22,23] using 2D layered semiconductors (WS_2 films),[24] and so on.[25−28] Unfortunately, many sensing materials in wearable sensors are unfriend to human skin, which is ignored in most of the time. Especially for breathing sensor, it is inevitable that small amounts of sensing materials are inhaled into the body, like lungs, causing various unexpected disease. Nevertheless, very limited toxicity data or safety precautions have been studied on the types of sensing materials for wearable application.[29−32]

Herein, hyperbranched polyethyleneimine (HPEI)-capped AuNPs, commonly used in the field of biomedicine, were selected for constructing well-designed biofriendly ultrathin 2D materials for flexible wearable devices, owing to their fine robustness, great biocompatibility, and almost nontoxicity.[33,34] Another moisture-sensitive elements was introduced using polydopamine (PDA), the adhesive proteins existed in mussels, chemically cross-linked with the HPEI/AuNPs to form extremely robust AuNPs-based monolayer. According to the literature, PDA functionalization can reduce the in vivo toxicity, implying that PDA is safe.[35] The as-designed freestanding 2D film exhibits strong interfacial cross-linking adhesion between sensing materials and elastic substrate, to avoid cracks and prevent chemical molecular escaping from substrate and inhaling into the lungs or human skin. In contrast to the conventional 2D materials, such a system plays a crucial role in the fast response process, and thus, it is expected to apply to circumstances where weak biological signals may change frequently. This kind of 2D sensing material based on nontoxic HPEI/AuNPs monolayer associated with biomimetic PDA, contains prominent electronic abilities, excellent photothermal performance, high surface-volume ratio, and absorption capacities. It thereby results in significant signal inductions during adsorbing water molecules on the surface of the thin film, which is quite sensitive for monitoring emotional changes and thus shows great potential in real-time health monitoring application.

EXPERIMENTAL SECTION

Materials. Hydrogen tetrachloroaurate trihydrate ($HAuCl_4 \cdot 3H_2O$, 99.99%) was purchased from Sigma-Aldrich. HPEI (M_w 10 000) and dopamine hydrochloride were purchased from Aladdin Ltd. (Shanghai China). All other reagents and solvents were of analytical reagent grade and received from Sinopharm Chemical Reagent.

Synthesis of HPEI/AuNPs. HPEI/AuNPs were prepared by reducing $HAuCl_4$ in the HPEI aqueous solution according to the literature with slight modifications.[36−39] Briefly, HPEI (69.4 mg) dissolved in deionized water (10 mL) was added with 153 μL of 0.1 M $HAuCl_4$ aqueous solution under vigorous magnetic stirring at 65 °C for 2 h. The resulting wine red solution was stored at 4 °C before use.

Formation of PDA/HPEI/AuNPs Film. First, 40 mg of dopamine hydrochloride dissolved in deionized water (15 mL) was added with 3 mL of the above HPEI/AuNPs solution and 2 mL of tris-buffer solution (100 mM, pH = 8.5). The solution was kept stable in an opened Petri-dish (diameter as 75 mm) and incubated in air for 12 h. A thin nanofilm can expect self-assembly at air/water interface. The freestanding films was subsequently transferred from the solution and washed with distilled water for further characterization.

Fabrication of PDA/HPEI/AuNPs Humidity Sensors. The PDA/HPEI/AuNPs film was transferred onto the surface of interdigitated Ni/Au interdigital electrode (IDE) which was sputter-deposited on the polyimide (PI) substrate (Ni: 3 μm thick; Au: 0.07 μm thick). The IDE pattern on the PI substrate provided an outline dimension of 6.5 mm × 15 mm. Typical dimensions of the interdigitated electrodes were 150 μm electrode width, 150 μm electrode separation, and 5.5 mm electrode length, and the number of electrodes was 21. The as-prepared sensor based on the PDA/HPEI/AuNPs film was connected to an electrochemical workstation or a light-emitting diode (LED) for further humidity testing experiments.

DOI: 10.1021/acsami.9b11918
ACS Appl. Mater. Interfaces 2019, 11, 36259−36269

Instrument. Ultraviolet−visible (UV−vis) absorption spectra were recorded with a TU-1810 spectrophotometer from Beijing Purkinje General Instrument Co. Ltd. in transmission mode. Transmission electron microscopy (TEM) was performed on a JEOL JEM-2100F instrument at 200 kV. Scanning electronic microscopy (SEM) measurements were carried out via a JEOL JMS-6700F scanning microscope. Atomic force microscopy (AFM) images were taken by a multimode AFM (Being Nano-Instruments, Ltd.) operating in the tapping mode using silicon cantilevers (spring constant: 3−40 N m^{-1}, resonant frequency: 75−300 kHz). The surface compositions and chemical states of the samples were analyzed by X-ray photoelectron spectroscopy (XPS) (AXIS ULTRA DLD, Kratos Analytical Ltd., Manchester, UK). XPS analysis was performed on a Shimadzu Axis scope, using Mg Kα as radiation resource. The photothermal performance of the PDA/HPEI/AuNPs devices was investigated using an 808 nm laser with the photo density of 2 W/cm^2 and an infrared (IR) thermal imaging system for temperature recording (MAG-V30, Wuhan VST Light & Technology Ltd.). The electrical impendence measurements were carried out using an electrochemical workstation (CHI660E). The controlled humidity environments were achieved in a constant temperature (~25 °C) and humidity room (~30%). The environment temperature and humidity were monitored by using a hygrometer (TESTO 608-H2). The humidity environments were achieved using saturated aqueous solutions of LiCl, $CaCl_2{\cdot}6H_2O$, $MgNO_3$, NaCl, and K_2SO_4 in a closed glass vessel at an ambient temperature of ~25 °C, which yielded approximately 29, 43, 54, 75, and 97% relative humidity (RH), respectively.

RESULTS AND DISCUSSION

A robust flexible humidity sensor with high sensitivity and ultrafast response was fabricated based on PDA-cross-linked-AuNP monolayer biomimetic nanofilm via a simple and low-cost interfacial assembly strategy (Figure 1A). The main contribution from PDA is to form a film via the interfacial polymerization process. PDA constitutes the bulk of the film by the interfacial polymerization and captures AuNPs during the polymerization and stacking process. The hydrophilic groups (e.g., −OH, $-NH_2$) can immediately "capture" water molecules through dynamical hydrogen bond interactions, showing remarkably high sensitivity for moisture monitoring (3 orders of magnitude). At the same time, the superior electronic and photothermal properties of AuNPs allow the sensor to "release" water molecules easily at low RH with high speed, leading to an ultrafast response and repeatable utilization. Therefore, this unique sensing material can be employed in wearable devices for real-time monitoring individual's health states by recording humidity signals from respiration and skin surface (Figure 1B,C). Interestingly, the designed sports watch is able to realize automatically visual display during daily exercise. In addition, the designed breathing mask was first used to detect emotional activities such as tension, crying, and laughing, which is promising in real-time monitoring of human emotions. Chemical cross-linking induced interfacial self-assembly suggests intriguing ability for the regeneration of the film at the cracked/damaged area, providing a powerful approach to successionally and repeatedly construct macroscopic freestanding 2D hybrid structures with monolayer nanoparticles. Such robust amphipathic films can be transferred to different liquid surfaces and solid substrates for achieving otherwise applications.

Fabrication and Characterization of PDA/HPEI/AuNPs Film. First, a chemical crosslinking-induced interfacial self-assembly was developed for preparing AuNP monolayer by virtue of interaction between PDA and HPEI-functional AuNPs (Figure 2A). AuNPs were prepared by using HPEI as both the reducing agent and stabilizer. The size of AuNPs is

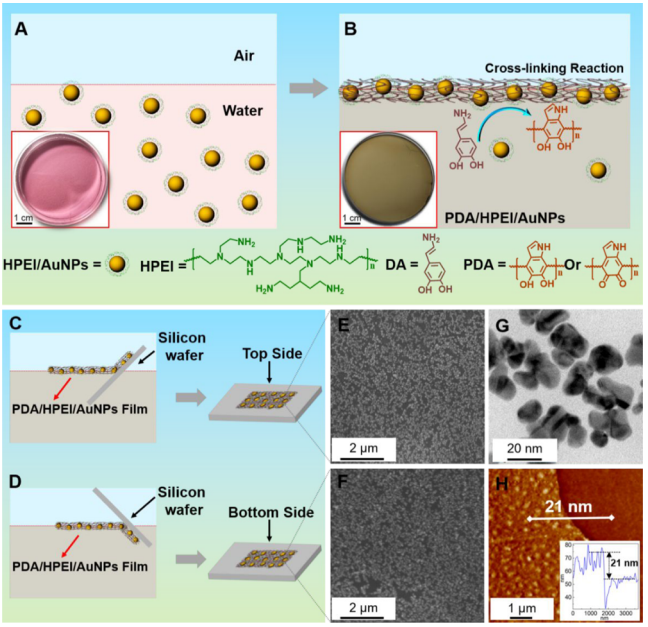

Figure 2. Synthesis and characterization of PDA/HPEI/AuNPs film (A) in situ reduction of $HAuCl_4$ into HPEI-functionalized AuNPs, (B) formation of oxygen-driven air/water interfacial polymerization of dopamine, which is cross-linked with HPEI/AuNPs. Transferring films with (C) top and (D) bottom sides onto silicon wafers. Representative SEM images of the (E) top and (F) bottom sides and (G) TEM and AFM images (H) of PDA/HPEI/AuNPs.

about 20 nm (Figure S1), displaying a pink color in low concentration (the inset in Figure 2A). The HPEI-functionalized AuNPs showed excellent stability and could disperse uniformly in dopamine alkaline solution. Under the acceleration of oxygen in air, dopamine molecules gradually self-polymerized into PDA and formed PDA thin films preferably at the air/water interface.[40,41] Meanwhile, as a result of the Michael addition reaction between amine groups in HPEI and catechol groups in PDA, HPEI on the surface of AuNPs can cross-link simultaneously with PDA chains during the interfacial formation of PDA films. Such interfacial behavior is in fact originated from dopamine and PDA. The key intermediate during the formation of PDA is 5,6-dihydroxyindole which exhibits amphiphilic behavior.[42] The role of PEI addition to the solution is to reinforce the overall mechanical properties of the interfacial film. This led to the implantation of AuNPs into the PDA film and successive interfacial assembly of PDA/HPEI/AuNPs (Figure 2B). With the increasing dopamine polymerization, the color of the dopamine solution changed gradually from pink to brown (inset in Figure 2B) and a macroscopic film with glossy reflection formed on the surface, indicating the formation of PDA/HPEI/AuNPs hybrid film. Unlike the uncontrollable size in traditional film, the size of macroscopic AuNPs film can be precisely tuned by simply adjusting the dimension of vessels in synthesis, leading to high reproducibility and repeatability. In addition, it was a green synthetic process because volatile organic solvents (e.g., toluene, pentanol, and hexane) usually used in traditional interface strategy[43−46] can be totally prevented.

DOI: 10.1021/acsami.9b11918
ACS Appl. Mater. Interfaces 2019, 11, 36259−36269

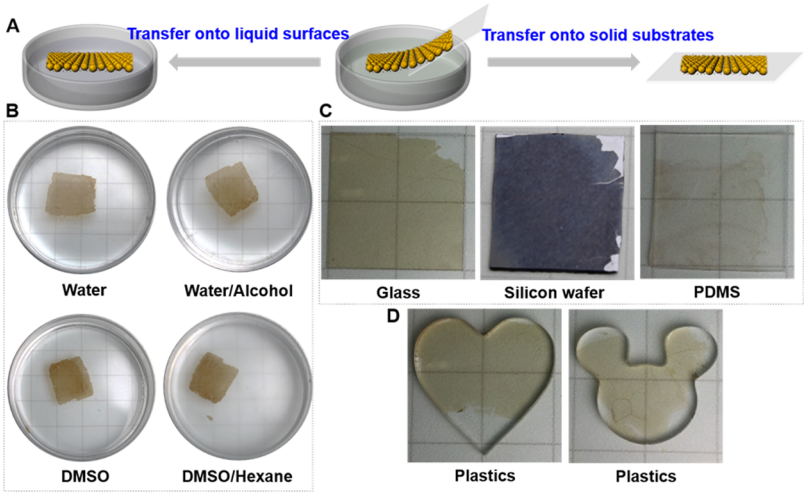

Figure 3. (A) Method for transferring films and photographs of AuNPs hybrid films on (B) liquid surfaces and (C,D) solid substrates.

In order to analyze the surface morphology and structures of PDA/HPEI/AuNPs films, their two sides were integrally transferred onto silica wafers (Figure 2C,D). On the top side, AuNPs closely packed and assembled into a uniform monolayer with a small fraction of voids (Figure 2E). From observation of top and bottom sides, the resultant film exhibited uniform structures in a large area. Dense AuNPs were evenly distributed in the film (Figure 2E,F). Higher and lower magnified images with both sides are characterized in Figure S2A−D, and the amplificatory image of the area was studied by TEM (Figures 2G and S2E), which confirmed that AuNPs were uniformly distributed in the monolayer film with various holes. To further characterize the obtained films, a cross-section of the sample transferred from the air/water interface onto a silica wafer was investigated by SEM (Figure S2F). It indicated that the film was composed of a single layer of AuNPs and spread uniformly. The thickness of the monolayer is about 21 nm from the cross-sectional SEM image and AFM (Figures S2F and 2H), near to the average size of HPEI/AuNPs (~20 nm). In addition, the AFM images clearly showed that AuNPs were immersed into a dopamine-polymerized system and tightly glued together, suggesting good mechanical properties.

The surface composition and structure of the as-prepared PDA/HPEI/AuNPs films were investigated by XPS spectrum (Figure S3). The as-prepared PDA/HPEI/AuNPs film contained Au, O, C, and N. Weight contents of Au, O, C, and N were determined to be 48.34, 27.38, 22.08, and 2.20% separately. C 1s peaks in Figure S3A were divided into four subpeaks corresponding to four types of carbon bonds.[47,48] The major peak at 284.7 eV is ascribed to the C−C or C═C bonds from the polymer backbone, while shoulders at 286.7 and 289.2 eV belong to the C−O and C═O bonds, respectively. The smallest subpeak at 285.2 eV corresponds to the C−N bonds. The Au 4f XPS spectra in Figure S3B display a double feature with peaks located at 87.8 and 84.4 eV, which is attributed to the Au $4f_{5/2}$ and $4f_{7/2}$ signals of metallic Au (Au^0), respectively.[25] The Au 4f peaks are relatively narrow and symmetrical, indicating only one chemical state of Au existing in PDA/HPEI/AuNPs film. The presence of nitrogen and oxygenate species was confirmed by the O 1s and N 1s XPS peaks as shown in Figure S3C,D.

Fourier transform IR (FTIR) was further used to study the composition and structure of the as-prepared PDA/HPEI/AuNPs film. The PDA absorption peaks are located at 1646 cm^{-1} (N−H) and 1298 cm^{-1} (C−N). It is a strong proof that PDA has cross-linked with AuNPs via the amine groups of HPEI (Figure S4). In order to optimize the close-packing density of AuNPs monolayer, a series of experiments were conducted by controlling the concentrations of AuNPs (0.033, 0.11, 0.23, 0.49 mM) and the resultant samples were characterized by TEM (Figure S5). When the concentration of AuNPs grows up, the density of AuNPs in the monolayer was gradually increased and then reached a saturate state. After that, the local aggregation and inhomogeneous distribution of AuNPs in the films would be found if the AuNP concentration experienced further increase. An optimal AuNP monolayer can be achieved by using 0.23 mM AuNPs. Larger particles will contribute to higher conductivity, but the thickness of the film will be increased and affect the responsive and recovery speed. In the future work, AuNPs with different size can be studied via a suitable method to modify them using HPEI, instead of the in situ reduction by HPEI. In this way, the size of AuNPs can be well controlled.

Owing to the stabilization of PDA film, the robust macroscopic film generated at the interface can be transferred facilely and integrally to liquid surfaces and solid substrates by Langmuir−Blodgett technology (Figure 3A), displaying perfect freestanding properties. Four types of liquid surfaces: water, dimethylsulfoxide (DMSO), water/alcohol, and DMSO/hexane were adopted here (Figure 3B). It can be seen that the as-transferred transparent AuNPs monolayer remains stable and compact after transferring to different liquid surfaces. A high mechanical stability was presented, unlike conventional interfacial AuNPs films hard to be transferred because of relatively weak physical interactions of interparticles (Figure S6). According to the literature[51,52] and the results in Figure 3, PDA (from adhesive proteins existed in mussels) can be transferred to almost all types of substrates, such as glass wafer, silicon wafer, flexible polydimethylsiloxane (PDMS), and plastics (Figure 3C,D). The ability of transferring the film to a patterned metal substrate allows us to readily produce various AuNPs patterns. Importantly the feasibility of transferring the film to flexible substrate presents its promising potential in wearable nanodevices. Moreover, such free-

DOI: 10.1021/acsami.9b11918
ACS Appl. Mater. Interfaces 2019, 11, 36259−36269

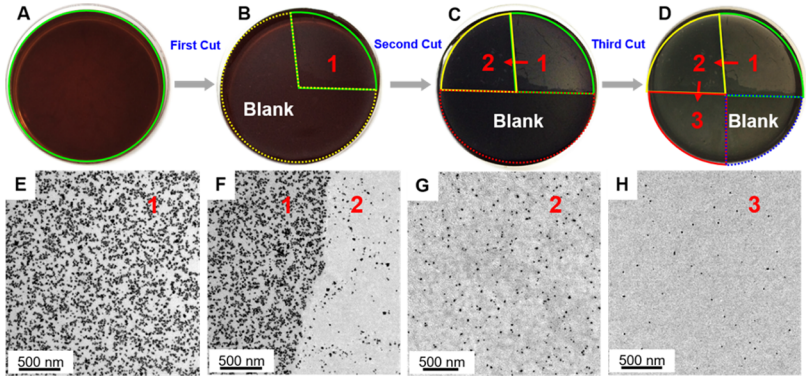

Figure 4. Regeneration properties of the film on newly exposed area by peeling damages. The "blank" denotes the newly exposed air/water interface, and "2" and "3" are the sequentially regenerated films every 3 h (A–D). Corresponding TEM images of the films of "1" (E), the interface between "1" and "2" (F), the film of "2" (G) and "3" (H).

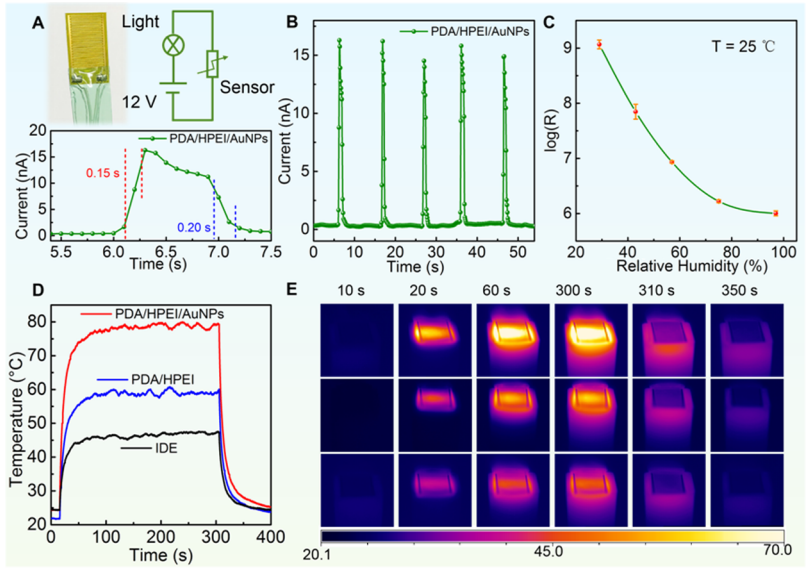

Figure 5. (A) Equivalent circuit and a photograph of the PDA/HPEI/AuNPs sensing element. The changes in the measured current from the film at 1 V as RH was switched between dry air (RH ≈ 25%) and humidity air (RH ≈ 45%). Estimated results showed the ultrafast response (0.15 s) and recovery (0.20 s) times. (B) Time-dependent response current from the film under 1 V bias voltage as RH was switched between the low level (25%) and high level (45%). (C) Derived RH-dependent resistance changes of the sensor. (D) Temperature variation and (E) IR thermal images of PDA/HPEI/AuNPs film, PDA/HPEI film, and the pure IDE substrate under a NIR laser (808 nm, 2 W/cm^2).

standing AuNPs can be cut into various shapes via different shapes of substrates. For example, "heart" and "mickey mouse" shapes of AuNPs monolayer were prepared simply by transferring onto the specific shaped plastic substrate. It is clear that the sensing material can be easily patterned with specific shapes to suit different positions of human body. The perfect adhesive property makes the as-prepared PDA/HPEI/AuNPs Film address the intrinsic problem, weak interaction between the traditional sensing materials, and targeted elastic substrate, in practical wearable sensing applications. Besides, the strong chemical adhesion between the PDA/HPEI/AuNPs film and elastic substrate enables avoiding cracks and preventing chemical molecular escaping from substrate and inhaling into the lungs or human skin.

More interestingly, because of the continuous interfacial polymerization of dopamine, the hybrid film can be regenerated repeatedly at air/water interface (Figure 4). Three-quarters of one fresh film was cut off to remain a quarter of the film (denoted as "1" highlighted by green line in Figure 4B). In this case, the dopamine self-polymerization in the blank area (highlighted by fellow dash lines) can proceed normally when the rest dopamine in solution was exposed to air. As expected, a new film was regenerated within 3 h at original area (denoted as "2" in the yellow dotted line, in Figure 4C). In addition, the newly formed film and the left old film amalgamated and composed a new compact film by robust adhesion. The semicircled area of the new film was cut again and labeled by yellow dash area in Figure 4C, and another new film was generated within subsequent 3 h again (denoted as "3" in the red dotted line, in Figure 4D). The robust attachment between the newly generated and the original film can also be clearly observed due to the intrinsic adhesive nature of PDA. It is extremely important for sensors to achieve the ability of self-healing and regeneration function in wearable devices applications.

The regenerative films at different growth stages were characterized by TEM (Figure 4E–H). The number of nanoparticles in region "2" reduced obviously compared with the region "1". There were two possible reasons: one was that many particles had transported to the interface for the

DOI: 10.1021/acsami.9b11918
ACS Appl. Mater. Interfaces 2019, 11, 36259–36269

formation of AuNP films; the other reason was that the rest HPEI/AuNPs may cross-link with free dopamine in the solution. Based on rough calculation, 45% of AuNPs in the initial solution was transported into the interfacial AuNPs film, which is much higher than the utilization rate of traditional method (11%).[49] Herein, this modified interfacial method also can be developed as a strategy for recovering noble metals from solutions for further applications.

RH Sensing/Photothermal Effect of PDA/HPEI/AuNPs Film. A PDA/HPEI/AuNPs film was employed to construct a series circuit (Figure 5A-top) for the investigation of RH-responsive electrical properties. The RH was controlled by the amount of moisture-nitrogen mixture. The response time is related to the structure of film (such as thickness and porosity), the variation, and change rate of humidity. Such ultrathin structures (high surface-volume ratio) can accelerate the adsorption and desorption of water molecules, to efficiently record dynamic signals from the surrounding environment. The thickness of our film is around 20 nm, when RH changes from 25 to 45%, the apparent current from 0.7 nA increased to 17 nA (Figure 5A,B), and the response and recovery times measured at the peak value up to 90% (Figure 5A-bottom) were 0.15 and 0.20 s, respectively. If we reduce the thickness of the film or the variation of the humidity, a shorter response time is expected to be obtained. During the humidity-sensing test, no obvious delay was observed. These results suggested that the device was humidity sensitive with a conductivity increase with humidity increase. The conductivity of the device was measured under different environmental humidity conditions with the increase of RH from 29 to 97%. The humidity environments were achieved using saturated aqueous solutions of LiCl, $CaCl_2{\cdot}6H_2O$, $MgNO_3$, NaCl, and K_2SO_4 in a closed glass vessel at an ambient temperature of ~25 °C, which yielded approximately 29, 43, 54, 75, and 97% RH, respectively. The resistance experienced changes almost 3 orders of magnitude in certain humidity range (from 29 to 97%) (Figure 5C). Thus, the lowest concentration that can be detected is 29%. Indeed, in this humidity-sensing process, water molecules were adsorbed onto the surface of the film, leading to an auto ionization reaction: $2H_2O \rightleftharpoons H_3O^+ + OH^-$. PDA and HPEI polymers contain a large number of amino ($-NH_2$) and hydroxyl groups ($-OH$) that induce the formation and cleavage of hydrogen bonds as wire or network with water molecules. This can rapidly connect the neighboring AuNPs and adsorb water molecules to form the electrical channels through the hydrogen bonds. Therefore, the hybrid film significantly increase the conductive pathway and result in greatly enhanced conductivity with the increase of RH. Dopamine derivatives with zhydrophilic group such as pyrogallol, as long as polymerization can occur, are expected to design as the humidity sensor.[50] To quantitatively characterize the humidity sensitivity of the device, the response at different RH levels was defined as response = $(R_{RH} - R_0)/R_0$, where R_{RH} and R_0 were the resistances of the device in dry air with the RH value reaching 97 and 29%, respectively. The maximum response value of the as-established device reached as high as 1245, indicating an excellent sensitivity to a high moisture environment.[24]

Temperature−time changes and thermal images were detected to study the photothermal performance of the PDA/HPEI/AuNPs films (Figure 5D,E). As expected, the PDA/HPEI/AuNPs film was quickly heated up and eventually achieved an equilibrium temperature around 79.5 °C within 100 s (Figure 5D), while the PDA/HPEI film and pure IDE substrate at plateau had only an equilibrium temperature of 58.2 and 46.3 °C, respectively. This clearly demonstrated that the PDA/HPEI/AuNPs film (1.37-fold-enhancement) owned a more efficient light-to-heat conversion than the PDA/HPEI film. Figure 5E shows the corresponding IR thermal images to study the AuNP effect on the photothermal performance of the film.[54,55] The photographs in the top line presents the IR thermal images of PDA/HPEI/AuNPs films, while the photographs in the middle line and bottom line link to the IR thermal images of PDA/HPEI films and the pure IDE substrate, respectively. After 300 s, the temperature decreased rapidly due to the fast thermal response to light on/off switching. Near IR (NIR) laser light, the color of PDA/HPEI/AuNPs films is much lighter than PDA/HPEI films and pure IDE substrate, suggesting better photothermal performance of the PDA/HPEI/AuNPs film.

Application as Sports Watch. Motivated by these outstanding properties of highly sensitive humidity sensing and great photothermal efficiency, the hybrid film was designed as an electronic device. The current of the circuit increased instantly once humid air was introduced, according to the green light of LED, as displayed in Figure 6A. The green light

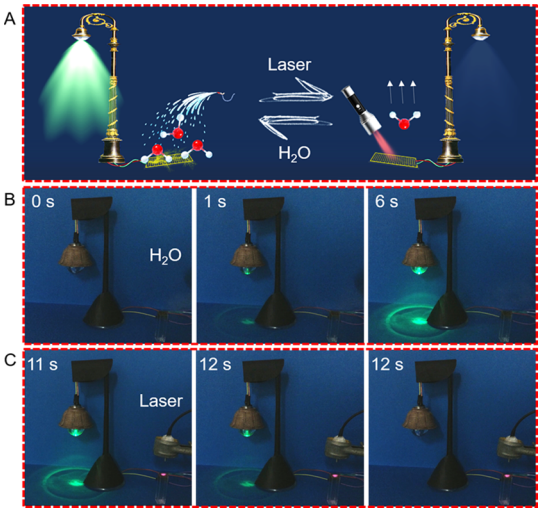

Figure 6. (A) Schematic and photographs of the PDA/HPEI/AuNP film as humidity sensor to (B) switch on/(C) off LED light (series circuit of IDE, 12 V battery and an LED).

of LED quickly disappeared under NIR illumination, which was contributed by rapid evaporation of water driven by light-to-heat conversion. Figure 6B displays the detailed changes of light intensity over introduced humid air. For the experiment of humid air continually stimulating the sensing material 6 s, the LED, at around 1 s, was lighted on after introducing the humid air. The light of LED started to become brighter as the wet air kept stimulating (Figure 6B). When time arrived at 6 s, the humid air stopped stimulating. From the 6th second to 10th second, negligible change of intensity was observed. A NIR laser was introduced at the 11th second. The light intensity decreased sharply to 0 within only 1 s under the NIR illumination (Figure 6C). Thus, clearly, the PDA/HPEI/AuNPs device exhibited excellent sensing performances with ultrafast response and very short recover times, good stability, and repeatability. At the same time, a PDA/HPEI film-based sensor with no AuNPs was also tested as a comparison (Figure

DOI: 10.1021/acsami.9b11918
ACS Appl. Mater. Interfaces 2019, 11, 36259−36269

S7). The recovery time of NIR-driven LED was nearly 38 times longer than that of the PDA/HPEI/AuNPs device. It can be concluded that a very better photothermal response of PDA/HPEI/AuNPs film than that of PDA/HPEI guaranteed a very shorter recovery time.

The hybrid film was employed into a flexible and wearable sports watch (Figure 7), which can be comfortably worn on

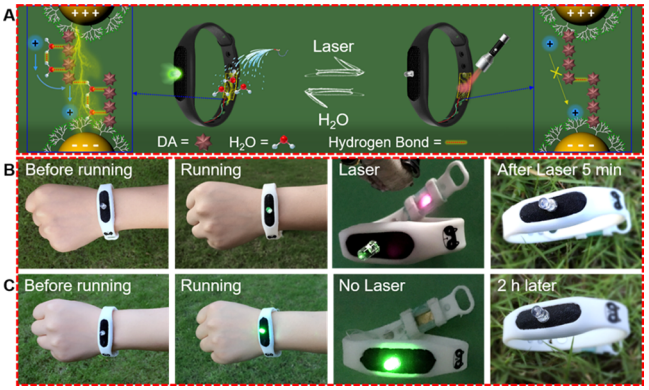

Figure 7. (A) Schematic and photographs of sports watch based on PDA/HPEI/AuNPs film recovering with laser (B) and without laser (C) (series circuit of IDE, 12 V battery and a LED).

human wrist to trace the perspiration. Abundant hydrophilic groups (−OH and $-NH_2$) in HPEI and PDA molecules acted as proton donors and acceptors and played a dominant part in stimulating the humidity sensor response.[20] At low humidity, ion transfer was difficult across the particles through proton hopping-transport and hardly to form conductive paths throughout the film because of the discontinuous adsorption of water molecules (Figure 7A-right). Evaporation of sweat from skin surface can be absorbed onto the surface of sensing material, and the RH around the sensing material will increase simultaneously. In this case, the Grotthuss mechanism probably occurred via formation and cleavage of hydrogen bonding network, allowing protons to hop between water molecules.[20] H_3O^+ was likely to produce charge carriers to serve as proton bridges to connect two AuNPs, which could contribute to an exponential enhancement in conductivity, and ultimately LED light was emitted (Figure 7A-left).

Figure 7B,C, respectively, presents the changes of the LED light before and after 10 min outdoor exercise. Normally, the moisture sensor is linked to temperature. In this paper, the sensor designed is insulated with skin by a 3 mm flexible PDMS frame and minimized the affect from the change of environmental temperature. It was so beneficial for visual perspiration monitoring. For the application of sports watches, the green LED began to show green light at the 6th minute of this 10 min running. When a 10 min running wearing sports watch was done, the PDA/HPEI/AuNPs sensing material was irradiated by a 808 nm laser for accelerating evaporation speed of water molecules. Interestingly, the lights went out quickly within 5 min (Figure 7B) because of the good photothermal performance of the PDA/HPEI/AuNPs film. Figure 7C shows that the lights need a longer time as 2 h to be off without NIR laser radiation when a 10 min running wearing sports watch was done. Based on the above results, the recovery time is related to the duration of the water stimulus. In the future, we can design breathable sports watch instead of the closed sports watch in this paper to accelerate the evaporation of moisture and thus accelerate the recovery time.

For the PDA/HPEI-based sensor, without the conductive and photothermal properties of AuNPs, a longer response time for the LED lighting and a higher value of recover time (~17 min/4 h with/without NIR illumination, respectively) were recorded (Figure S8A,B). In addition, this sports watch can be employed as a real-time perspiration monitor indoor exercise

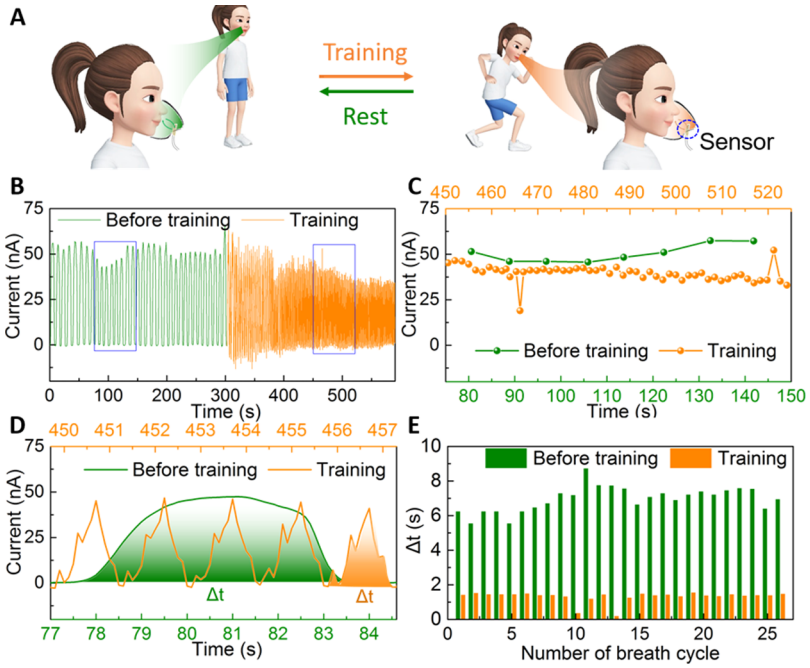

Figure 8. (A) Schematic illustration of humidity sensor for human breath monitoring before training (left) and during training (right). (B) Real-time breathing analysis, (C) respiratory amplitude, (D) estimated time of a breath cycle, and (E) the time of every breath cycle when a subject before training and during training.

DOI: 10.1021/acsami.9b11918
ACS Appl. Mater. Interfaces 2019, 11, 36259−36269

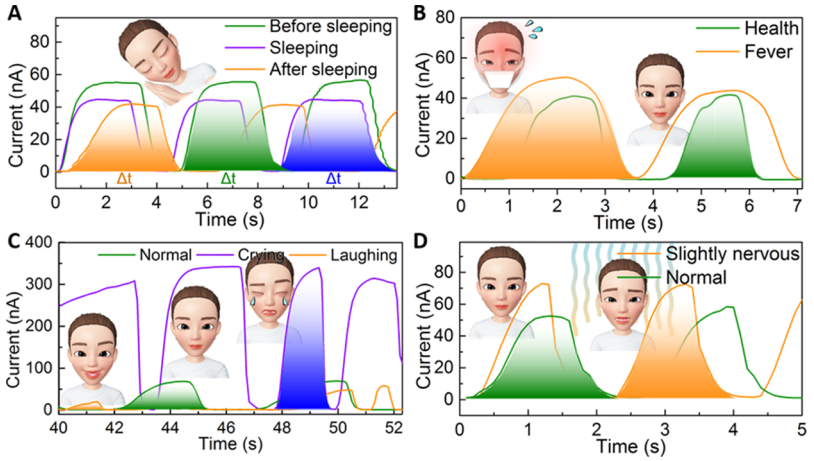

Figure 9. Simultaneous humidity flow sensing from the smart breathing monitoring mask device. Real-time breathing analysis with estimated time of a breath cycle when a subject is at different physical and emotional activation (A) sleeping, (B) different health states, (C) crying and laughing, and (D) slightly nervous state.

by connecting to computer (Figure S9). It was evident that the sensor with AuNPs (green line) achieved more than 5 times the current compared to PDA/HPEI (red line). The current recovery time of PDA/HPEI/AuNPs was around 17 min simultaneously, near twice as fast as that of PDA/HPEI (~32 min). Through the data collection and analysis, such wearable PDA/HPEI/AuNP sensor also showed fast response and superior recover ability for the function of efficient visual or real-time health monitoring. To study the excellent stability of our sensor-based sports watch, after thousands of repetitive experiments and 6 months of placement, the sports watch was again used to detect the LED light with RH changes. As shown in the Figure S10, the results make clear that the water absorption still can light on the LED through the obtained humidity sensor.

Based on the ultrafast response and highly sensitive performance, the hybrid film can be used as a powerful noninvasive tool for continuously monitoring human breath. Because of a higher humidity of exhaled air than the inhaled (ambient) air, human breath can be recorded by monitoring the variations in the RH values.[21] Here, a modified breath mask was fabricated (Figure 8A). With individual breathing out into the mask through the nose, the RH fleetly rose as soon as the exhaled flow reached the sensor and rapidly declined to ambient value during inhaling. The test object breathed comfortably on wearing the sensing mask. The signals with normal breathing rate were collected consistently (around 5 min), and the current was nearly repetitive in breathing cycles (Figure 8B, green line). A reasonably narrow change of amplitude can be seen in Figure 8C (green line), probably from normal respiratory fluctuations. Then, the volunteer started to do mild indoor training for 5 min, and the subsequent breathing signals were recorded simultaneously (Figure 8B, orange line). A slow decline in the current value in the respiratory amplitude was observed in Figure 8C (orange line), which was likely to occur as the exercise induced dehydration owing to perspiration and felt thirsty. For a more accurate study, the breath time from the output breathe curve of every breath cycle was further calculated (Figure 8D), displaying around 5 fold fast breathing speed during training in contrast to normal states. The statistical data also displayed the average breath time before and during training, about 7 and 1.4 s, respectively (Figure 8E).

Interestingly, the breathing signals at different physiological (e.g., sleeping, fever) and emotional states (e.g., crying, laughing, and nervous) were first recorded. The signals were clearly revealed by different breath RH levels (Figures 9 and S11), very possibly caused by different metabolic processes and respiratory controlling. Figures 9A and S11A show breathing relatively steady in the sleeping process, before, during, and after sleeping. The current dropped by a third after falling into sleep, implying that the RH level decreased during sleeping. More importantly, it needs to be pointed out that a new breathing state called "fast breathing" occurred around 25 min in during sleeping state. This may be arising when the brain condition performs "rapid eye movement (REM) sleep" at that time. An automatic nerve was disarray (e.g., breathing and blood pressure unsteadies) at the state of "REM sleep".[53] In Figures 9A and S11B, the time of every breath cycle during sleeping was slightly faster, compared to that of normal breath before or after sleeping. The breathing curves obtained from fever states (Figures 9B and S11C) demonstrated that the breathing at cold states was disorder with higher RH level. The time of every breath cycle was calculated, indicating that the time of every breath cycle at cold states took around 1.7-fold longer than the time at the healthy state (Figure S11D).

More interestingly, the mask can be developed for observing physiological response specificity in emotions including negative (e.g., anger, anxiety, fear, crying) and positive (happiness, laughing) emotions (Figures 9C,D and S11E–H). Physiological activities at sad situations (negative emotion) would increase cardiovascular sympathetic controlling and change respiratory activity.[56] When the breath was characterized during crying activities, it was found that breathing through the nose presented a dramatic increase (~4.6-fold) of the respiratory amplitude compared to normal states (Figures 9C and S11E). Here, the reason may be that tear was formed by tear glands and was delivered toward the upper respiratory tract, and then, the humidity of breathing flow increased. Another reason was probably that water from the internal body fluid was transferred to the respiratory system when emotion emerged, caused by the warm, humidified breathing. These results revealed that the great fluctuations of amplitude increased with irregular respiratory activities, particularly during crying process. Further, the time of every breath cycle was calculated (Figure 9C), which

DOI: 10.1021/acsami.9b11918
ACS Appl. Mater. Interfaces 2019, 11, 36259−36269

displayed that moisture of respiratory airflow significantly ascended during crying while slightly decreased during laughing compared to normal states. Emotions were identified by more irregular and faster breathing, as evidenced in the fluctuations of time of every breath cycle (Figure S11F). 0.33 cycle/s during crying and 0.25 cycle/s during laughing were recorded compared to 0.17 cycle/s at normal states (calculated from Figure S11E). Nervous symptoms can lead to the increase and fluctuation of breath frequency (Figure S11G). The calculated time (Figures 9D and S11H) implied that the shortness of breathing was induced by slightly nervous.

In this paper, the test results only reflect an individual, and the obtained signals vary from person to person. Figure S12 demonstrates the current−time (I−t) curves from different volunteers varied among healthy adult males and females. Therefore, this wearable device can be applied in a customized monitoring system and continuously provide an individual's daily health information in long-term monitoring. On the other hand, more detailed research in this area should combine with more data collection and deep learning to analyze the performance in the future. Note that dozens of volunteers in the process of respiratory monitoring did not suffer from any allergic reaction, which supported our sensing material of good safety from another aspect. Such a sensing mask should be significant in breathing analysis because it can provide a simple and powerful noninvasive strategy for diagnosing diseases such as asthma, sleep apnea syndrome, or other respiratory diseases.

CONCLUSIONS

We presented a simple strategy to fabricate a 2D sensing material based on the PDA-cross-linked-AuNPs monolayer. Around 45% of nanoparticles could be assembled from solution into a 2D monolayer AuNPs film (around 4-fold in contrast to traditional interface method). The hybrid structure was adhered directly and facilely to a flexible IDE substrate for realizing highly sensitive humidity-sensing application. More importantly, this system is greatly biocompatible and totally nontoxic, unlike many controversial sensing materials about safety issues. The sensor reached a maximum resistance response of almost 3 orders of magnitude toward moisture over a wide range (RH from 29 to 97%, 25 °C). Such device integrated the advantages of AuNPs (high surface-volume ratio, highly conductible and photothermal performance) with the moisture absorption capacities in the hydrophilic group of polymers through dynamical hydrogen bond interactions to achieve a humidity-sensing ability. The sensor-based wearable sports watch was finely designed to detect the RH change on human skin surface for visually physiological monitoring application. Moreover, the ultrafast response sensor of breathing mask was employed effectively for real-time monitoring of human breath at different physical states, such as training, sleeping and cold states, and even emotional monitoring system including crying, laughing, and nervous state. The new and safe concept of wearable sensor would be promising in customizable and reusable real-time health monitoring and the inexpensive biological detection. The freestanding, adhesive, and regenerative characteristics endow the hybrid film with many other specials functions, like self-healing and arbitrary patterning, which is of significance in wearable applications.

ASSOCIATED CONTENT

Supporting Information

The Supporting Information is available free of charge on the ACS Publications website at DOI: 10.1021/acsami.9b11918.

UV−vis, XPS, FTIR spectra, TEM, SEM images of PDA/HPEI/AuNPs, and relevant data for humidity-sensing devices (PDF)

AUTHOR INFORMATION

Corresponding Authors

*E-mail: yjhuang@hznu.edu.cn (Y.H.).
*E-mail: xuqing.liu@manchester.ac.uk (X.L.).
*E-mail: tao.chen@nimte.ac.cn (T.C.).

ORCID

Youju Huang: 0000-0001-5815-9784
Linxi Hou: 0000-0002-7962-0936
Xuqing Liu: 0000-0001-5998-6546
Tao Chen: 0000-0001-9704-9545

Notes

The authors declare no competing financial interest.

ACKNOWLEDGMENTS

We gratefully acknowledge the National Natural Science Foundation of China (grant no. 51873222), the Fujian Province-Chinese Academy of Sciences STS project (2017T31010024), the Youth Innovation Promotion Association of the Chinese Academy of Science (2016268), and the Key Research Program of Frontier Science and Education of Chinese Academy of Sciences (QYZDB-SSW-SLH036).

REFERENCES

(1) Gao, W.; Emaminejad, S.; Nyein, H. Y. Y.; Challa, S.; Chen, K.; Peck, A.; Fahad, H. M.; Ota, H.; Shiraki, H.; Kiriya, D.; Lien, D.-H.; Brooks, G. A.; Davis, R. W.; Javey, A. Fully Integrated Wearable Sensor Arrays for Multiplexed in Situ Perspiration Analysis. *Nature* **2016**, *529*, 509−514.

(2) Yan, Y.; Warren, S. C.; Fuller, P.; Grzybowski, B. A. Chemoelectronic circuits based on metal nanoparticles. *Nat. Nanotechnol.* **2016**, *11*, 603−608.

(3) Cai, Y.; Shen, J.; Dai, Z.; Zang, X.; Dong, Q.; Guan, G.; Li, L. J.; Huang, W.; Dong, X. Extraordinarily Stretchable All-Carbon Collaborative Nanoarchitectures for Epidermal Sensors. *Adv. Mater.* **2017**, *29*, 1606411.

(4) He, J.; Xiao, P.; Lu, W.; Shi, J.; Zhang, L.; Liang, Y.; Pan, C.; Kuo, S.-W.; Chen, T. A Universal High Accuracy Wearable Pulse Monitoring System via High Sensitivity and Large Linearity Graphene Pressure Sensor. *Nano Energy* **2019**, *59*, 422−433.

(5) Trung, T. Q.; Duy, L. T.; Ramasundaram, S.; Lee, N.-E. Transparent, Stretchable, and Rapid-Response Humidity Sensor for Body-Attachable Wearable Electronics. *Nano Res.* **2017**, *10*, 2021−2033.

(6) Wile, D. J.; Ranawaya, R.; Kiss, Z. H. Smart watch accelerometry for analysis and diagnosis of tremor. *J. Neurosci. Methods* **2014**, *230*, 1−4.

(7) Tao, L.-Q.; Zhang, K.-N.; Tian, H.; Liu, Y.; Wang, D.-Y.; Chen, Y.-Q.; Yang, Y.; Ren, T.-L. Graphene-Paper Pressure Sensor for Detecting Human Motions. *ACS Nano* **2017**, *11*, 8790−8795.

(8) Yan, H.; Zhang, L.; Yu, P.; Mao, L. Sensitive and Fast Humidity Sensor Based on A Redox Conducting Supramolecular Ionic Material for Respiration Monitoring. *Anal. Chem.* **2017**, *89*, 996−1001.

(9) An, B. W.; Heo, S.; Ji, S.; Bien, F.; Park, J. U. Transparent and flexible fingerprint sensor array with multiplexed detection of tactile pressure and skin temperature. *Nat. Commun.* **2018**, *9*, 2458.

DOI: 10.1021/acsami.9b11918
ACS Appl. Mater. Interfaces 2019, 11, 36259−36269

(10) Yin, B.; Liu, X.; Gao, H.; Fu, T.; Yao, J. Bioinspired and Bristled Microparticles for Ultrasensitive Pressure and Strain Sensors. *Nat. Commun.* **2018**, *9*, 5161.
(11) Kang, J.; Son, D.; Wang, G. N.; Liu, Y.; Lopez, J.; Kim, Y.; Oh, J. Y.; Katsumata, T.; Mun, J.; Lee, Y.; Jin, L.; Tok, J. B.; Bao, Z. Tough and Water-Insensitive Self-Healing Elastomer for Robust Electronic Skin. *Adv. Mater.* **2018**, *30*, No. e1706846.
(12) Lochner, C. M.; Khan, Y.; Pierre, A.; Arias, A. C. All-Organic Optoelectronic Sensor for Pulse Pximetry. *Nat. Commun.* **2014**, *5*, 5745.
(13) Joh, H.; Lee, S.-W.; Seong, M.; Lee, W. S.; Oh, S. J. Engineering the Charge Transport of Ag Nanocrystals for Highly Accurate, Wearable Temperature Sensors through All-Solution Processes. *Small* **2017**, *13*, 1700247.
(14) Ruzsanyi, V.; Baumbach, J. I.; Sielemann, S.; Litterst, P.; Westhoff, M.; Freitag, L. Detection of Human Metabolites Using Multi-Capillary Columns Coupled to Ion Mobility Spectrometers. *J. Chromatogr. A* **2005**, *1084*, 145−151.
(15) Han, D.-D.; Zhang, Y.-L.; Ma, J.-N.; Liu, Y.; Mao, J.-W.; Han, C.-H.; Jiang, K.; Zhao, H.-R.; Zhang, T.; Xu, H.-L.; Sun, H.-B. Sunlight-Reduced Graphene Oxides as Sensitive Moisture Sensors for Smart Device Design. *Adv. Mater. Technol.* **2017**, *2*, 1700045.
(16) Wang, X.; Xiong, Z.; Liu, Z.; Zhang, T. Exfoliation at the Liquid/Air Interface to Assemble Reduced Graphene Oxide Ultrathin Films for a Flexible Noncontact Sensing Device. *Adv. Mater.* **2015**, *27*, 1370−1375.
(17) Borini, S.; White, R.; Wei, D.; Astley, M.; Haque, S.; Spigone, E.; Harris, N.; Kivioja, J.; Ryhänen, T. Ultrafast graphene oxide humidity sensors. *ACS Nano* **2013**, *7*, 11166−11173.
(18) Miao, J.; Cai, L.; Zhang, S.; Nah, J.; Yeom, J.; Wang, C. Air-Stable Humidity Sensor Using Few-Layer Black Phosphorus. *ACS Appl. Mater. Interfaces* **2017**, *9*, 10019−10026.
(19) Erande, M. B.; Pawar, M. S.; Late, D. J. Humidity Sensing and Photodetection Behavior of Electrochemically Exfoliated Atomically Thin-Layered Black Phosphorus Nanosheets. *ACS Appl. Mater. Interfaces* **2016**, *8*, 11548−11556.
(20) He, J.; Xiao, P.; Shi, J.; Liang, Y.; Lu, W.; Chen, Y.; Wang, W.; Théato, P.; Kuo, S.-W.; Chen, T. High Performance Humidity Fluctuation Sensor for Wearable Devices via a Bioinspired Atomic-Precise Tunable Graphene-Polymer Heterogeneous Sensing Junction. *Chem. Mater.* **2018**, *30*, 4343−4354.
(21) Mogera, U.; Sagade, A. A.; George, S. J.; Kulkarni, G. U. Ultrafast Response Humidity Sensor Using Supramolecular Nanofibre and its Application in Monitoring Breath Humidity and Flow. *Sci. Rep.* **2015**, *4*, 4103.
(22) Lee, J.; Mulmi, S.; Thangadurai, V.; Park, S. S. Magnetically Aligned Iron Oxide/Gold Nanoparticle-Decorated Carbon Nanotube Hybrid Structure as a Humidity Sensor. *ACS Appl. Mater. Interfaces* **2015**, *7*, 15506−15513.
(23) Zhou, G.; Byun, J.-H.; Oh, Y.; Jung, B.-M.; Cha, H.-J.; Seong, D.-G.; Um, M.-K.; Hyun, S.; Chou, T.-W. Highly Sensitive Wearable Textile-Based Humidity Sensor Made of High-Strength, Single-Walled Carbon Nanotube/Poly(vinyl alcohol) Filaments. *ACS Appl. Mater. Interfaces* **2017**, *9*, 4788−4797.
(24) Guo, H.; Lan, C.; Zhou, Z.; Sun, P.; Wei, D.; Li, C. Transparent, Flexible, and Stretchable WS_2 Based Humidity Sensors for Electronic Skin. *Nanoscale* **2017**, *9*, 6246−6253.
(25) Ju, D.-X.; Xu, H.-Y.; Qiu, Z.-W.; Zhang, Z.-C.; Xu, Q.; Zhang, J.; Wang, J.-Q.; Cao, B.-Q. Near Room Temperature, Fast-Response, and Highly Sensitive Triethylamine Sensor Assembled with Au-Loaded ZnO/SnO_2 Core-Shell Nanorods on Flat Alumina Substrates. *ACS Appl. Mater. Interfaces* **2015**, *7*, 19163−19171.
(26) Yan, H.; Guo, S.; Wu, F.; Yu, P.; Liu, H.; Li, Y.; Mao, L. Carbon Atom Hybridization Matters: Ultrafast Humidity Response of Graphdiyne Oxides. *Angew. Chem., Int. Ed. Engl.* **2018**, *57*, 3922−3926.
(27) Late, D. J.; Huang, Y.-K.; Liu, B.; Acharya, J.; Shirodkar, S. N.; Luo, J.; Yan, A.; Charles, D.; Waghmare, U. V.; Dravid, V. P.; Rao, C. N. R. Sensing Behavior of Atomically Thin-Layered MoS_2 Transistors. *ACS Nano* **2013**, *7*, 4879−4891.
(28) Erande, M. B.; Pawar, M. S.; Late, D. J. Humidity Sensing and Photodetection Behavior of Electrochemically Exfoliated Atomically Thin-Layered Black Phosphorus Nanosheets. *ACS Appl. Mater. Interfaces* **2016**, *8*, 11548−11556.
(29) Nel, A.; Xia, T.; Mädler, L.; Li, N. Toxic potential of materials at the nanolevel. *Science* **2006**, *311*, 622−627.
(30) Kostarelos, K.; Bianco, A.; Prato, M. Promises, facts and challenges for carbon nanotubes in imaging and therapeutics. *Nat. Nanotechnol.* **2009**, *4*, 627−633.
(31) Kostarelos, K. The long and short of carbon nanotube toxicity. *Nat. Biotechnol.* **2008**, *26*, 774−776.
(32) Bianco, A. Graphene: safe or toxic? The Two Faces of the Medal. *Angew. Chem., Int. Ed. Engl.* **2013**, *52*, 4986−4997.
(33) Song, W.-J.; Du, J.-Z.; Sun, T.-M.; Zhang, P.-Z.; Wang, J. Gold nanoparticles capped with polyethyleneimine for enhanced siRNA delivery. *Small* **2010**, *6*, 239−246.
(34) Gu, S.; Ma, K.; Kong, J.; Al-Ghanim, K. A.; Mahboob, S.; Liu, Y.; Zhang, X. Functionalized Polyethyleneimine-gold Nanoparticles-Porphyrin Nanocomposite for Electrochemical Glucose Biosensing. *Int. J. Electrochem. Sci.* **2017**, *12*, 5092−5103.
(35) Hong, S.; Kim, K. Y.; Wook, H. J.; Park, S. Y.; Lee, K. D.; Lee, D. Y.; Lee, H. Attenuation of the in Vivo Toxicity of Biomaterials by Polydopamine Surface Modification. *Nanomedicine* **2011**, *6*, 793−801.
(36) Wen, S.; Zheng, F.; Shen, M.; Shi, X. Synthesis of polyethyleneimine-Stabilized Gold Nanoparticles for Colorimetric Sensing of Heparin. *Colloids Surf., A* **2013**, *419*, 80−86.
(37) Zhao, W.; Jia, W.; Sun, M.; Liu, X.; Zhang, Q.; Zong, C.; Qu, J.; Gai, H. Colorimetric Detection of Cu^{2+} by Surface Coordination Complexes of Polyethyleneimine-Capped Au Nanoparticles. *Sens. Actuators, B* **2016**, *223*, 411−416.
(38) Cho, T. J.; Pettibone, J. M.; Gorham, J. M.; Nguyen, T. M.; MacCuspie, R. I.; Gigault, J.; Hackley, V. A. Unexpected Changes in Functionality and Surface Coverage for Au Nanoparticle PEI Conjugates: Implications for Stability and Efficacy in Biological Systems. *Langmuir* **2015**, *31*, 7673−7683.
(39) Sun, X.; Dong, S.; Wang, E. One-step preparation of highly concentrated well-stable gold colloids by direct mix of polyelectrolyte and $HAuCl_4$ aqueous solutions at room temperature. *J. Colloid Interface Sci.* **2005**, *288*, 301−303.
(40) Zhang, L.; Xiao, P.; Lu, W.; Zhang, J.; Gu, J.; Huang, Y.; Chen, T. Macroscopic Ultrathin Film as Bio-Inspired Interfacial Reactor for Fabricating 2D Freestanding Janus CNTs/AuNPs Hybrid Nanosheets with Enhanced Electrical Performance. *Adv. Mater. Interfaces* **2016**, *3*, 1600170.
(41) Hong, S.; Schaber, C. F.; Dening, K.; Appel, E.; Gorb, S. N.; Lee, H. Air/Water Interfacial Formation of Freestanding, Stimuli-Responsive, Self-Healing Catecholamine Janus-Faced Microfilms. *Adv. Mater.* **2014**, *26*, 7581−7587.
(42) Ponzio, F.; Payamyar, P.; Schneider, A.; Winterhalter, M.; Bour, J.; Addiego, F.; Krafft, M.-P.; Hemmerle, J.; Ball, V. Polydopamine Films from the Forgotten Air/Water Interface. *J. Phys. Chem. Lett.* **2014**, *5*, 3436−3440.
(43) Hu, L.; Chen, M.; Fang, X.; Wu, L. Oil-Water Interfacial Self-Assembly: a Novel Strategy for Nanofilm and Nanodevice Fabrication. *Chem. Soc. Rev.* **2012**, *41*, 1350−1362.
(44) Li, Y.-J.; Huang, W.-J.; Sun, S.-G. A universal approach for the self-Assembly of Hydrophilic Nanoparticles into Ordered Monolayer Films at a Toluene/Water Interface. *Angew. Chem., Int. Ed. Engl.* **2006**, *45*, 2537−2539.
(45) Xia, H.; Wang, D. Fabrication of Macroscopic Freestanding Films of Metallic Nanoparticle Monolayers by Interfacial Self-Assembly. *Adv. Mater.* **2008**, *20*, 4253−4256.
(46) Lu, X.; Huang, Y.; Liu, B.; Zhang, L.; Song, L.; Zhang, J.; Zhang, A.; Chen, T. Light-Controlled Shrinkage of Large-Area Gold Nanoparticle Monolayer Film for Tunable SERS Activity. *Chem. Mater.* **2018**, *30*, 1989−1997.

DOI: 10.1021/acsami.9b11918
ACS Appl. Mater. Interfaces 2019, 11, 36259−36269

(47) Zhang, Z.; Huang, J.; Yuan, Q.; Dong, B. Intercalated graphitic carbon nitride: a fascinating two-dimensional nanomaterial for an ultra-sensitive humidity nanosensor. *Nanoscale* **2014**, *6*, 9250−9256.
(48) Tao, Y.; Dandapat, A.; Chen, L.; Huang, Y.; Sasson, Y.; Lin, Z.; Zhang, J.; Guo, L.; Chen, T. Pd-on-Au Supra-nanostructures Decorated Graphene Oxide: An Advanced Electrocatalyst for Fuel Cell Application. *Langmuir* **2016**, *32*, 8557−8564.
(49) Park, Y.-K.; Yoo, S.-H.; Park, S. Assembly of Highly Ordered Nanoparticle Monolayers at a Water/Hexane Interface. *Langmuir* **2007**, *23*, 10505−10510.
(50) Wang, Y.; Park, J. P.; Hong, S. H.; Lee, H. Biologically Inspired Materials Exhibiting Repeatable Regeneration with Self-Sealing Capabilities without External Stimuli or Catalysts. *Adv. Mater.* **2016**, *28*, 9961−9968.
(51) Chen, L.; Lu, M.; Wang, Y.; Huang, Y.; Zhu, S.; Tang, J.; Zhu, C.; Liu, X.; Yin, W. Whole System Design of a Wearable Magnetic Induction Sensor for Physical Rehabilitation. *Adv. Intell. Syst.* **2019**, *1*, 1900037.
(52) Lee, H.; Lee, B. P.; Messersmith, P. B. A Reversible Wet/Dry Adhesive Inspired by Mussels and Geckos. *Nature* **2007**, *448*, 338−341.
(53) Akita, S.; Seki, A.; Watanabe, K. A Monitoring of Breathing Using a Hetero-Core Optical Fiber Sensor. *Proc. SPIE* **2011**, *7981*, 79812W.
(54) Feng, J.; Chen, L.; Xia, Y.; Xing, J.; Li, Z.; Qian, Q.; Wang, Y.; Wu, A.; Zeng, L.; Zhou, Y. Bioconjugation of Gold Nanobipyramids for SERS Detection and Targeted Photothermal Therapy in Breast Cancer. *ACS Biomater. Sci. Eng.* **2017**, *3*, 608−618.
(55) Zeng, L.; Pan, Y.; Zou, R.; Zhang, J.; Tian, Y.; Teng, Z.; Wang, S.; Ren, W.; Xiao, X.; Zhang, J.; Zhang, L.; Li, A.; Lu, G.; Wu, A. 808 nm-Excited Upconversion Nanoprobes with Low Heating Effect for Targeted Magnetic Resonance Imaging and High-Efficacy Photodynamic Therapy in HER2-Overexpressed Breast Cancer. *Biomaterials* **2016**, *103*, 116−127.
(56) Kreibig, S. D. Autonomic Nervous System Activity in Emotion: A Review. *Biol. Psychol.* **2010**, *84*, 394−421.

DOI: 10.1021/acsami.9b11918
ACS Appl. Mater. Interfaces 2019, 11, 36259−36269